Human embryonic stem cell-derived neurons adopt and regulate the activity of an established neural network

Jason P. Weick[a,1], Yan Liu[a], and Su-Chun Zhang[a,b,c,d,e]

[a]Waisman Center, [b]Neuroscience Training Program, Departments of [c]Neuroscience and [d]Neurology, and [e]School of Medicine and Public Health, University of Wisconsin–Madison, 647 Waisman Center, Madison, WI 53705

Edited by Fred H. Gage, The Salk Institute, San Diego, CA, and approved October 19, 2011 (received for review May 26, 2011)

Whether hESC-derived neurons can fully integrate with and functionally regulate an existing neural network remains unknown. Here, we demonstrate that hESC-derived neurons receive unitary postsynaptic currents both in vitro and in vivo and adopt the rhythmic firing behavior of mouse cortical networks via synaptic integration. Optical stimulation of hESC-derived neurons expressing Channelrhodopsin-2 elicited both inhibitory and excitatory postsynaptic currents and triggered network bursting in mouse neurons. Furthermore, light stimulation of hESC-derived neurons transplanted to the hippocampus of adult mice triggered postsynaptic currents in host pyramidal neurons in acute slice preparations. Thus, hESC-derived neurons can participate in and modulate neural network activity through functional synaptic integration, suggesting they are capable of contributing to neural network information processing both in vitro and in vivo.

AMPA | cortical neurons | GABA

Embryonic stem cells (ESCs) (1, 2) and induced pluripotent stem cells (iPSCs) (3–5) can be directed to regional- and transmitter-specific neuronal subtypes (6–13), which correct the behavioral deficits associated with disease phenotypes in animal models after transplantation (9, 10, 14, 15). It is generally believed that functional integration into existing circuitry is required for their long-term therapeutic potential. Both mouse (m) ESC- and hESC-derived neurons express basic functional properties, such as action potential (AP) firing and synaptic currents (6, 11, 16, 17). In addition, when deposited on the dentate gyrus of organotypic hippocampal slice cultures, they display postsynaptic responses upon stimulation of perforant path fibers (18, 19). Similarly, in acute slice preparations from transplanted animals, hESC- and human iPSC-derived neurons demonstrate spontaneous postsynaptic currents (PSCs) (16, 20) that are thought to be derived from presynaptic transmitter release from host neurons. Thus, in vitro-generated neurons can generate APs in response to current injection and can receive unitary synaptic inputs from surrounding neurons.

However, complete functional integration requires more complex physiological properties, including PSC-induced spiking, presynaptic outputs to surrounding neurons, and the ability to regulate the behavior of a preexisting neural network. Because of technological deficiencies in stimulating groups of neurons simultaneously, none of these properties has been definitively demonstrated for ESC-derived neurons from either mouse or human. In this study, we used optogenetic targeting of hESC-derived neurons (21, 22) to test these capabilities in vitro and in vivo. First, we exploited the unique bursting pattern of activity in mouse cortical cultures to demonstrate that hESC-derived neurons not only adopt bursting behavior but can also modulate the mouse network activity via synaptic output. Furthermore, we show that human neurons make both excitatory and inhibitory synaptic connections with individual mouse neurons. Lastly, we demonstrate that hESC-derived neurons can elicit PSCs in hippocampal pyramidal neurons in slices taken from transplanted mouse brains.

Results

hESC-Derived Neurons Adopt the Bursting Behavior of Mouse Cortical Networks via Synaptic Integration. To address whether hESC-derived neurons can fully integrate with an established neural network, we first used long-term cocultures with mouse cortical neurons from embryonic day 16 pups. A unique feature of these cultures is the presence of synchronized network activity referred to as "bursting" (Fig. 1*C*, *i*) (23, 24), which may arise from deafferentation because of limited numbers of tonically active neurons (25). Bursting has not been reported in hESC-derived neuron cultures (6, 17, 22), which continuously add tonically active neurons from progenitor cells when differentiated to a "default" dorsal forebrain phenotype (6, 17, 22). These cultures are primarily comprised of both glutamatergic and GABAergic neurons when plated alone or in coculture (6, 22) (Fig. S1 *A* and *B*).

Current-clamp recordings from GFP-labeled mouse neurons cultured alone (Fig. 1*A*, *Left*) revealed the presence of spontaneous bursting as early as 7 d in vitro (div) (Fig. S2*A*, upper trace), which persisted for the duration of the experiment (Fig. S2*A*, lower trace). We thus considered cortical cultures that displayed bursting to qualify as an established neural network. For cocultures, we plated whole hESC-derived neuroepithelial aggregates (21div) onto 7div mouse cultures. These aggregates contain dividing neural progenitors, as well as postmitotic neurons expressing Channelrhodopsin-2 (ChR2)-mCherry (Fig. 1*A*, *Right*). Table S1 illustrates that, compared with measurements for human neurons, mouse neurons demonstrated significantly larger capacitance ($P < 0.001$, $n = 4$), lower input resistance (R_{in}; $P < 0.001$, $n = 4$), and more hyperpolarized resting membrane potentials (RMPs) ($P < 0.001$, $n = 4$) at each time point. Furthermore, mouse neurons had larger inward and outward voltage-gated currents at all times tested (Fig. 1*B*; 8-wk time point shown).

Similar to previous studies, current-clamp recordings from hESC-derived neurons plated alone (Fig. 1*A*, *Center*) showed no bursting activity after 6 wk of culture (Fig. 1*C*, *ii*) or at any time point recorded (2 wk: 0 of 242; 4 wk: 0 of 211; 6 wk: 0 of 67; 8 wk: 0 of 53). In contrast, human neurons in coculture with mouse cortical neurons displayed prominent bursting activity in coculture (Fig. 1*C*, *iii* and *iv*, and *E*). Importantly, bursting measured in current-clamp mode is indicated by AP generation (Figs. 1*C* and 2 and Figs. S1*B* and S4). However, we also use bursting generally to refer to any synchronized postsynaptic activity measured in voltage-clamp, regardless of whether summation currents were observed. Because hESC-derived neurons demonstrated progressively hyperpolarized RMPs during the study period (Table S1), we quantified the proportion of bursting cells

Author contributions: J.P.W. and S.-C.Z. designed research; J.P.W. performed research; Y.L. contributed new reagents/analytic tools; J.P.W. analyzed data; and J.P.W. and S.-C.Z. wrote the paper.

The authors declare no conflict of interest.

This article is a PNAS Direct Submission.

[1]To whom correspondence should be addressed. E-mail: jasonweick@gmail.com.

This article contains supporting information online at www.pnas.org/lookup/suppl/doi:10.1073/pnas.1108487108/-/DCSupplemental.

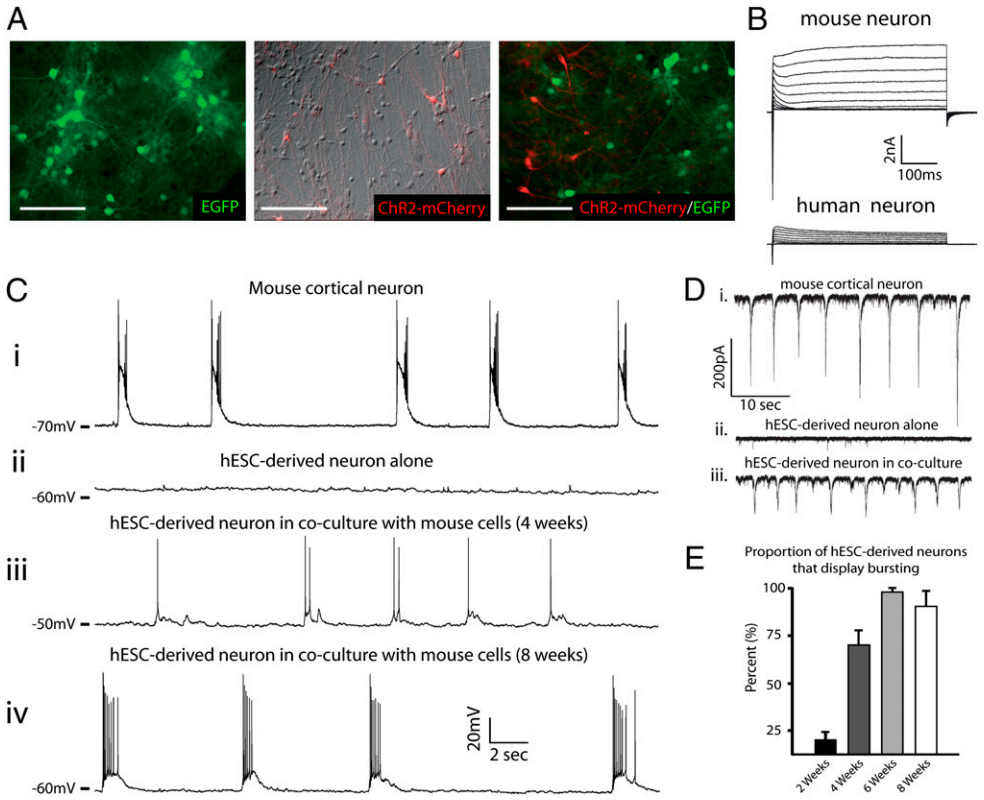

Fig. 1. hESC-derived neurons adopt the bursting activity of a preexisting neural network. (*A*) Differential interference contrast and/or epifluorescent images of mouse cortical cultures (*Left*), hESC-derived neuronal cultures (*Center*), or mouse-human cocultures (*Right*) after 4 wk in vitro. (*B*) Representative traces of mouse (*Upper*) or human neuron (*Lower*) that received 500-ms voltage steps from −50 to +50 mV at 8 wk of coculture. (*C*) Representative current-clamp recordings from a mouse or human neurons at various time points. Bursting activity was routinely observed in mouse neurons (*i*) and human neurons between 4 (*iii*) and 8 wk (*iv*) of coculture, whereas no bursting was observed in hESC-derived cultures alone (*ii*). (*D*) Recordings in voltage-clamp display similar results as those in current-clamp but provide a uniform driving force (−70-mV holding potential) for quantification of the proportion of bursting cells. (*E*) Pooled data demonstrate a progressive increase in the proportion of hESC-derived neurons that display bursting at various times in coculture. Data are means ± SEM. (Scale bars, 100 μm.)

using voltage-clamp at a holding potential of −70 mV. Under these conditions, we still observed bursting behavior in mouse (Fig. 1*D*, *i*) and human (Fig. 1 *D*, *ii*) neurons in coculture but not in human neurons alone (Fig. 1*D*, *ii*). Fig. 1*E* illustrates that bursting was observed in few hESC-derived neurons in coculture for 2 wk, a majority of cells at 4 wk, and nearly all neurons after 6 and 8 wk of coculture. Interestingly, human cells displayed significantly smaller burst amplitudes than mouse neurons (Fig. S3 *A* and *B*), even when corrected for differences in cell size (Fig. S3*C*). Lastly, we observed the presence of "superbursts" (25) in both mouse (Fig. S2*B*, upper trace) and cocultured human (Fig. S2*B*, lower trace) neurons, which exhibited long-duration depolarizations lasting multiple seconds with regenerative spiking. Thus, hESC-derived neurons can develop synchronized bursting activity but only in the presence of an established mouse cortical network.

To determine whether bursting activity in human neurons was attributable to functional integration with the existing mouse network (and not a newly generated human network), we used dual patch-clamp recording of neurons of both species cocultured for 6 and 8 wk. Fig. 2 *A* and *B* illustrates the presence of nearly simultaneous bursting in a mouse (upper trace) and hESC-derived neuron (lower trace) when bursts were spontaneously generated by the culture. Similar results were obtained from two mouse neurons that also displayed simultaneous bursting (Fig. S4). All dual recordings in which both cells displayed bursting (n = 9) also demonstrated simultaneous bursting. Interestingly, activity in the mouse cell generally preceded that of the human cell by a mean duration of 61.4 ± 9.5 ms (Fig. 2*B*; range: −1.8–410.1 ms). Furthermore, all bursts recorded in both mouse and human neurons were eliminated by the application of the AMPA receptor antagonist 6-cyano-7-nitroquinoxaline-2, 3-dione (CNQX) (Fig. 2*F*; 50 μM). Thus, hESC-derived neurons became part of the existing cortical network via excitatory synaptic integration.

hESC-Derived Neurons Regulate the Excitability of an Existing Mouse Cortical Network via Synaptic Output. We next asked whether human neurons could influence mouse network activity via synaptic output. A train of 10 light pulses delivered at 10 Hz to specifically activate hESC-derived neurons was sufficient to induce spiking in the human cell (Fig. 2 *C* and *D*, lower trace) and bursting behavior in the mouse neuron (Fig. 2 *C* and *D*, upper trace). Light-induced bursting was highly repeatable (Fig. 2*C*), and light-induced APs (LI-APs) in hESC-derived neurons preceded bursting activity in mouse cells by a mean duration of 73.7 ± 6.2 ms (range: 38.2–107.9 ms; Fig. 2*D*, see below). Furthermore, light-induced bursting mimicked the spontaneous bursting activity even when applied within seconds of a spontaneous burst (Fig. 2*E*). We hypothesized that light-induced bursting was attributable to multiple hESC-derived neurons simultaneously triggering PSCs in mouse cells. Indeed, in mouse cells in which light stimulation did not induce bursting, multiple PSCs were triggered immediately following the light pulse (Fig. S5*A*). In addition, dual patch-clamp recordings from two human neurons revealed simultaneous excitation upon light stimulation (Fig. S5*B*). Thus, human neurons are capable of regulating overall

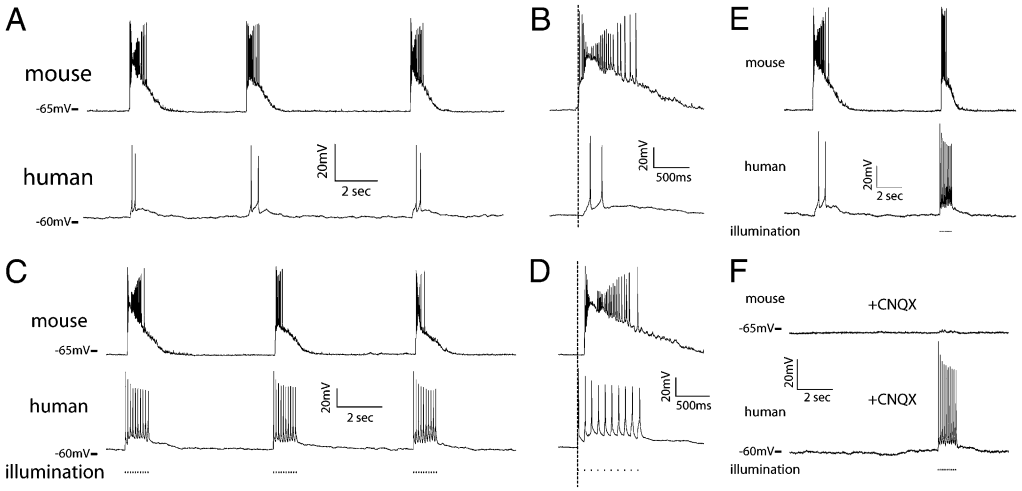

Fig. 2. hESC-derived neurons display a reciprocal synaptic relationship with dissociated mouse cortical cultures. (*A*) Dual patch-clamp recordings from mouse (upper trace) and human (lower trace) that display repeatable, nearly simultaneous bursting in both cells when bursts were generated spontaneously by the culture. (*B*) Expanded time scale demonstrates that mouse activity preceded human activity (mean: 61.4 ± 9.5 ms). (*C*) Repeated 10-Hz light stimulations produced APs in hESC-derived neurons (*Lower*) and coincident bursting activity in mouse neurons (*Upper*). (*D*) Expanded time scale demonstrates that the first light stimulus preceded bursting by a mean duration of 73.7 ± 6.2 ms. (*E*) Dual patch-clamp recordings from a human (*Upper*) and mouse (*Lower*) neuron in which a spontaneous burst was triggered by the culture, followed by a light-induced burst generated by human neurons. (*F*) All spontaneous bursts and light-induced bursts (but not light-induced APs) were eliminated by application of CNQX (50 μM).

network activity, likely via synaptic output of multiple human neurons firing simultaneously in response to optical stimulation.

As mentioned, spontaneous and light-induced bursts were eliminated by application CNQX, whereas LI-APs remained (Fig. 2*F*). However, in some dual recordings (two of nine), light-induced PSCs (LI-PSCs) were observed in the mouse neuron after application of CNQX (Fig. 3*A*). A 1-Hz light stimulus was still able to trigger escaped action currents in the human cell (Fig. 3 *A* and *B*, upper traces), as well as individual PSCs in the mouse neuron that had relatively long-duration decay constants ($\tau = 20.2 \pm 1.7$ ms; Fig. 3*B*, middle trace). LI-PSCs in these pairs occurred with a mean delay from light onset of 13.9 ± 1.2 ms (range: 9.7–20.2 ms) and 4.0 ± 0.5 ms from AP onset (range: 1.1–6.6 ms). Furthermore, these currents were completely blocked by picrotoxin (50 μM), suggesting that they were GABAergic in nature (Fig. 3 *A* and *B*, lower traces).

Similar results were found in multiple mouse neurons recorded alone where a current–voltage (I-V) relationship revealed a mean reversal potential of −41 ± 2.7 mV (Fig. 3*C*), in good agreement with the reversal potential of chloride for the solutions used (−44 mV). In cultures lacking high-frequency PSCs, we were also able to detect LI-PSCs in mouse cells with faster kinetics ($\tau = 4.1 \pm 0.7$ ms; Fig. 3*D*), indicative of excitatory PSCs. In the presence of the NMDA receptor antagonist D-2-amino-5-phosphonopentanoic acid (AP5) (25 μM), a I-V relationship curve revealed a reversal potential of 2.6 ± 0.7 mV, close to the reversal potential for AMPA receptors. Under these conditions, LI-PSCs in mouse neurons occurred after a mean delay of 17.7 ± 1.4 ms from light onset (range: 9.7–32.8 ms). Fig. 3*E* demonstrates the increase in percentage of mouse neurons that displayed evidence of LI-PSCs, which reached 31.5 ± 5% by 8 wk in coculture. Although the fraction of LI-PSCs observed did not significantly change between 6 and 8 wk ($P = 0.32$, $n = 4$), incidence at these time points was significantly greater than the 4-wk time point (Fig. 3*E*; $P = 0.02$, $n = 4$). However, the incidence frequency determined may underestimate the percentage of synaptically connected cells because of the high degree of spontaneous activity in many of the mouse neurons (Fig. S6), which made LI-PSCs difficult to resolve in some cases. Taken together, hESC-derived neurons regulate mouse network excitability via excitatory (glutamatergic) and/or inhibitory (GABAergic) synaptic connections.

hESC-Derived Neurons Make Functional Synapses with Mouse Neurons in Vivo. To determine whether hESC-derived neurons could form functional presynaptic connections with mouse neurons in vivo, we transplanted neuroepithelial aggregates infected with Syn-ChR2(H134R)-mCherry to the CA3 region of 2-mo-old SCID ($n = 32$) mice. The hippocampus was chosen because of its highly organized structure such that endogenous neurons could be readily identified without additional labeling. In 50-μm slices taken from perfused animals, many highly arborized mCherry$^+$ neurons that coexpressed the human nuclear antigen (Fig. S7) could be seen migrating through various strata of CA3, CA1, and dentate gyrus (Fig. 4*A*). For physiological analysis, we performed acute coronal slice preparations (400 μm) to maximize the opportunity of maintaining intact projections from transplanted neurons. All mCherry$^+$ cells ($n = 12$) displayed inward and outward voltage-gated currents, as well as spiking (Fig. 4*B*), in response to current injection. Furthermore, a majority of hESC-derived neurons (8 of 12) demonstrated spontaneous PSCs, indicating their postsynaptic integration within the slice (Fig. 4*C*). In all cases ($n = 12$), light stimuli triggered spikes when cells were held at endogenous RMPs, and most (9 of 12) could reliably generate LI-APs up to 10 Hz (Fig. 4*D*).

Mouse neurons recorded near mCherry$^+$ processes (Fig. 4*E*) displayed typical passive and active properties of pyramidal neurons (Fig. 4*F*) and generated trains of accommodating APs in response to current injection (Fig. 4*G*). In a minority of cells (3 of 91), LI-PSCs could be triggered in a repeatable fashion (Fig. 4*H*, *i*, upper trace) but with variable amplitudes (mean amplitude: 36.6 ± 2.4 pA; range: 11.1–61.7 pA). All displayed similar kinetics to inhibitory PSCs detected in cultures (Fig. 4*I*, upper trace; compare with Fig. 3*B*; $\tau = 16.9 \pm 0.9$ ms), occurred with a mean delay from light onset of 27.1 ± 2.4 ms and were blocked by application of 50 μM picrotoxin (Fig. 4 *H* and *I*, lower traces of each pair). Thus, following transplantation, grafted human neurons could reciprocally interact with the host neuronal network via pre- and postsynaptic integration. Interestingly, although a majority of neurons in hESC-derived dorsal forebrain

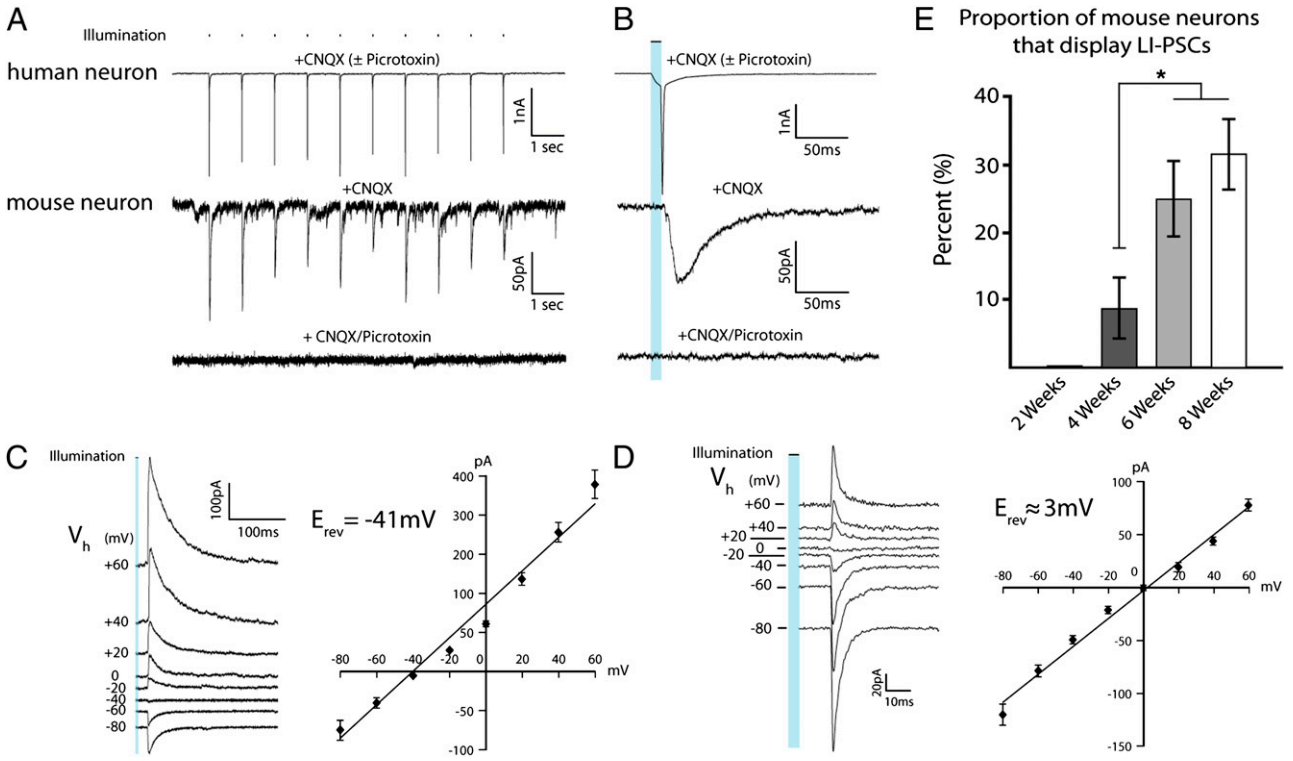

Fig. 3. hESC-derived neurons act as presynaptic neurons within an existing neural network. (*A*) Traces from individual human (*Upper*) and mouse (*Lower*) neurons recorded in the presence of CNQX (50 μM) after coculture for 8 wk. Light stimulation of 1 Hz triggered escaped action currents in a hESC-derived neuron and unitary PSCs in a mouse neuron (middle trace), which could be blocked by application of the $GABA_A$ receptor antagonist picrotoxin (50 μM; lower trace). (*B*) Expanded time scale illustrates the close temporal relationship among light stimulus, action current, and PSC. Note that traces from the human cell were essentially the same in the presence of CNQX alone or CNQX plus picrotoxin. (*C*) Representative traces from a mouse neuron recorded alone showing relatively long decay constants (τ = 20.2 ± 1.7 ms) and I-V relationship demonstrating a reversal potential of −41 ± 2.7 mV. (*D*) Representative traces from a mouse neuron recorded alone in the presence of AP5 (25 μM) showing relatively short decay constants (τ = 4.1 ± 0.7 ms) and I-V relationship demonstrating a reversal potential of 2.6 ± 0.7 mV. (*E*) Pooled data revealed a progressive increase in proportion of mouse neurons that displayed light-induced postsynaptic currents. Data are means ± SEM (*$P < 0.05$).

cultures are likely glutamatergic (6, 17) (Fig. S1), our findings suggest that inhibitory neurons may functionally integrate more readily after transplantation.

Discussion

Here, we used optogenetic technology to definitively demonstrate that hESC-derived neurons are capable of complete synaptic integration with a preexisting network both in vitro and in vivo, and can modulate the excitability of a network via synaptic output. In coculture with bursting mouse cortical neurons, hESC-derived neurons progressively adopted the same bursting behavior, whereby network-derived activation of human neurons led to depolarization and spiking behavior. We verified that the human neurons were part of the existing network via dual patch-clamp recording and that bursting in human cells was driven by synaptic activity via antagonism of glutamatergic neurotransmission. Furthermore, optical stimulation of $ChR2^+$ human neurons caused excitatory and inhibitory postsynaptic responses in mouse neurons and could trigger bursting behavior. Lastly, activation of $ChR2^+$ human neurons in slices taken from transplanted mouse brains revealed light-induced PSCs in pyramidal neurons.

The integration of hESC-derived neurons within an established network displays interesting parallels with the incorporation of nascent dentate granule cells (DGCs) in mature hippocampus. Newly born DGCs in the subgranular zone display physiological properties distinct from mature cells, such as elevated RMPs, high R_{in}, reduced thresholds for long-term potentiation and depression (26, 27), and potentially increased excitability (28). hESC-derived neurons exhibit similarly depolarized RMPs, higher R_{in} (Table S1) (6), and potentially increased excitability even after extended time periods (22). It will be interesting to know whether these properties are critical for integration and whether hESC-derived neurons display comparable synaptic plasticity characteristics to those of immature DGCs. Secondly, postsynaptic maturation, indicated by robust dendritic spine growth of newly born DGCs, occurs 3–4 wk after terminal differentiation (29). Our results demonstrate a significantly greater proportion of bursting cells (i.e., postsynaptically mature) after 4 wk compared with the 2-wk time point (Fig. 1*E*). Furthermore, it is thought that DGCs require 1–2 mo of maturation to fully integrate with the established circuitry in the hippocampus (28, 30, 31). Here, integration of hESC-derived neurons occurred over a similar time course, where significantly greater presynaptic integration (Fig. 3*E*) was observed after 6–8 wk than at earlier time points.

A similar time course is observed for the improvements in behavioral symptoms of neurodegeneration after stem cell transplantation, supporting the idea that synaptic integration is crucial for long-term outcomes of cell replacement in disease models (32). Significant effects of transplanted dopamine (DA) neurons on rotational behavior in Parkinson models are not typically observed at 4 wk after transplantation but are observed after 6–8 wk (7, 14), consistent with our findings for presynaptic innervation (Fig. 3*E*). In addition to the temporal correlation, hESC-derived neurons are capable of integrating synaptic

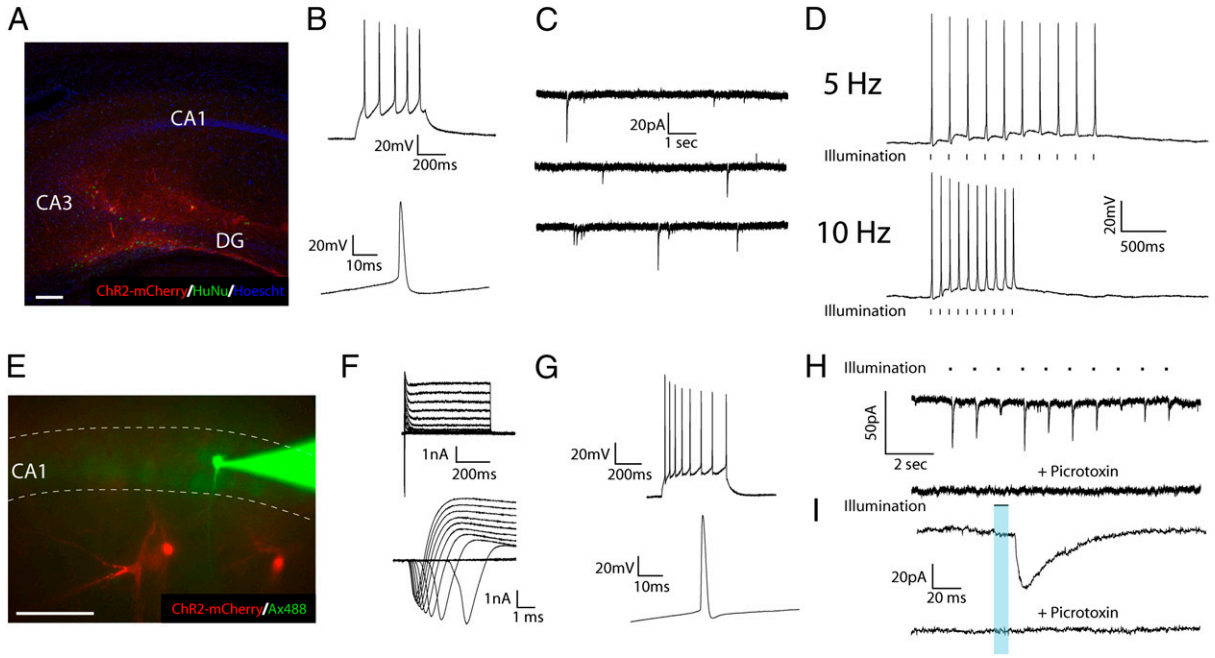

Fig. 4. hESC-derived neurons regulate the excitability of host neurons following transplantation. (*A*) Fluorescent image of a mouse brain section in which transplanted ChR2-expressing hESC-derived neurons have been stained with human nuclear antigen and can be seen innervating various regions of the hippocampus. (*B*) Representative current-clamp recordings in a ChR2-mCherry^{+} neuron showing a single (*Lower*) and a 10-Hz train (*Upper*) of non-accommodating APs in response to 70 pA of current injection. (*C*) Sequential voltage-clamp traces from a hESC-derived neuron that demonstrates the presence of spontaneous PSCs. (*D*) Current-clamp traces demonstrating the presence of light-induced APs at 5 Hz (*Upper*) and 10 Hz (*Lower*). (*E*) Fluorescent image of acute hippocampal slice containing ChR2-mCherry hESC-derived neurons (red) in close proximity to a recorded CA1 pyramidal neuron loaded with alexafluor-488 (green). (*F*) Voltage-clamp traces of CA1 pyramidal neuron demonstrating inward and outward currents (lower trace: expanded time scale for clarity of inward currents). (*G*) Current-clamp recordings of CA1 neuron showing a single (*Lower*) and a train (*Upper*) of accommodating APs in response to 70 pA of current injection. (*H*) Voltage-clamp recording of CA1 neuron that demonstrates the presence of repeatable light-induced PSCs (upper trace) that were blocked by picrotoxin (50 μM; lower trace). (*I*) Expanded time scale of currents in *H* illustrating the relatively long decay constants of LI-PSCs ($\tau = 20.2 \pm 1.7$ ms). (Scale bars, 100 μm.)

currents to produce spiking (Fig. 1*C*), can make excitatory and inhibitory connections with mouse neurons (Fig. 3 *C* and *D*), and pre- and postsynaptically integrate in vivo (Fig. 4). Although these data suggest that hESC-derived neurons may participate in network information processing, future research is necessary to demonstrate a causal link between synaptic integration and the behavioral changes observed after transplantation.

The combination of directed neural differentiation of ESCs and iPSCs with optogenetics may have broad utility for evaluating the physiological mechanisms underlying outcomes of stem cell transplants. Similar to previous studies that examined synaptic connectivity between brain regions (33, 34), ChR2 expression could be used to map local and distant neuronal connections between transplanted and endogenous neurons in disease models. In vivo, the use of implantable light-stimulation devices (35) will give researchers unprecedented real-time access to examine the physiological underpinnings of successful cell replacement for neurodegenerative disorders. For instance, whereas the forebrain glutamatergic or GABAergic neurons used in this study may be useful for treatment of frontotemporal dementia, ischemia, or epilepsy, optogenetics can be used to target a number of potentially therapeutic populations such as midbrain DA neurons (7, 8) and spinal motor neurons (13). These methods may be particularly necessary to interrogate more subtle, modulatory effects of metabotropic transmitters such as DA (36), which has been the focus of many neuronal cell-replacement studies (37). The ability to stimulate multiple neurons simultaneously (Fig. S4) could allow for detection of the downstream consequences of DA release, such as its effect on sodium currents (38). This would allow for a direct demonstration of presynaptic integration of transplanted DA neurons, which has been historically difficult using traditional techniques (39).

Materials and Methods

Cell Culture and Transplantations. Animal experiments were carried out according to the protocols approved by the University of Wisconsin–Madison Animal Care and Use Committee. Mouse cortical neurons (embryonic days 14.5–16.5) were provided by Dr. E.W. Dent (University of Wisconsin–Madison), cultured according to previously published methods (40), and plated at a density of 5×10^5 cells/10-mm coverslip. hESCs (WA09; passages 24–35) were cultured and differentiated to neurons essentially as described previously (6), with the addition of B27 (1:100; Invitrogen), 37.5 mM NaCl, and 0.3% glucose to differentiation media (DM). For cocultures, four to five hESC-derived neuroepithelial aggregates (21div) were plated onto 7div mouse cultures.

For transplantation experiments, SCID mice (8-10 wk of age) were anesthetized with 1% isoflurane mixed with oxygen and received 2 μL of 35div to 40div cell suspension (~5×10^5 cells/μL) unilaterally to the CA3 region of the hippocampus using the following stereotaxic coordinates: anterior–posterior = −2.46 mm; left–right lateral = ±2 mm; and dorsoventral = −2.25 mm. Three to 4 mo following transplantation, mice were either killed for sectioning and staining according to previously published methods (15) or were prepared for ex vivo recordings.

Lentiviral Vectors and Transduction. Channelrhodopsin-2 constructs used were either the *Syn-ChR2-mCherry* described previously (22) or *Syn-ChR2(H134R)-mCherry* transfer vector created using methods described previously (41), by replacing the *CamKIIα* promoter with the *synapsin-1* promoter. Lentiviral production and transduction, as well as the pGK-GFP lentivirus, have been described previously (42). Viral particles were concentrated by ultracentrifugation (SW28 rotor; Beckman Coulter) at 20,000 × *g* for 3 h, resuspended in DM and titrated using the Lenti-X qRT-PCR kit (Clontech). hESC-derived aggregates or 12-mm coverslips containing mouse neurons were incubated

with respective viruses (10^6 transducing units/mL) for 24 h and then washed with DM.

Immunochemical Staining. Immunolabeling of hESC-derived neurons was performed according to previously established methods (6, 15) using the following primary antibodies: polyclonal DsRed (1:1,000; Millipore), monoclonal β_{III}-Tubulin (1:1,000; Sigma), polyclonal GABA (1:1,000; Sigma), and a human-specific nuclear antibody (1:400; Millipore). To detect primary antibodies, we used Alexa-Fluor secondary antibodies (1:1,000; Jackson ImmunoResearch) conjugated to fluorophores FITC, Cy3, and Cy5, which were visualized using a Nikon confocal workstation (D-Eclipse C1) running EZ-C1 software (version 3.5). 3D reconstruction and surface rendering were performed using Imaris software (version 7.3; Bitplane).

Electrophysiological Recordings and Light Stimulation. Whole cell patch-clamp recordings were performed as previously described (22), with the following modifications. The extracellular solution was a modified HBSS that contained (in mM) 120 NaCl, 3 KCl, 2 $CaCl_2$, 1 $MgCl_2$, 15 Hepes, and 23 glucose (pH 7.4, 300 mOsm). The intracellular recording solution contained the following (in mM): 121 K-gluconate, 22 KCl, 10 Na^+-Hepes, 10 EGTA, and 4 Mg-ATP (pH 7.2, 290 mOsm). Pharmacological antagonists picrotoxin (50 μM), CNQX (50 μM), and AP5 (25 μM; Sigma) were applied using a gravity-fed drug barrel system or bath applied via extracellular solution. The number of neurons recorded at each time point ranged from 12 to 30 for each group (human and mouse). Acute slices from transplanted SCID mice were prepared according to previously published methods (22), using the intracellular solution described above.

Light stimulation was achieved by a custom-built LED device that used a ~950-mW blue light-emitting diode (LED) (470 nm; Thor Labs) coupled to a fiber optic cable that was placed 2–5 mm from ChR2-expressing neurons. Power to the LED was delivered through a current-controlled LED driver (Thor Labs). Light intensity could be modulated by a potentiometer and ranged from 0.1 to 1 mW/mm^2, with most stimulations using ~0.4 mW/mm^2. Triggered light pulses were controlled via the open source Arduino microcontroller platform (SmartProjects) with timing (high time and frequency) regulated by custom Arduino programs.

Statistical Analyses. One-way ANOVA followed by Newman–Keuls post hoc tests were used to determine whether mean differences between groups were different and were considered significant when $P < 0.05$. Data are reported as means ± SEM.

ACKNOWLEDGMENTS. We thank Erik W. Dent for providing mouse cortical cultures; Justin C. Williams and Tom Richner for support with our LED stimulation device; the Laboratory for Optical and Computational Instrumentation (LOCI), Kevin Eliceiri, Johannes Schindelin, and Jimmy Fong for assistance with 3D reconstructions; and Eva D. Zarnowska for helpful discussions. This study was supported by National Institutes of Neurological Diseases and Stroke Grants NS045926, NS057778, and RNS074281A and, in part, by National Institutes of Health Core Grant P30 HD03352 (to the Waisman Center from the National Institute of Child Health and Human Development).

1. Evans MJ, Kaufman MH (1981) Establishment in culture of pluripotential cells from mouse embryos. *Nature* 292:154–156.
2. Thomson JA, et al. (1998) Embryonic stem cell lines derived from human blastocysts. *Science* 282:1145–1147.
3. Yu J, et al. (2007) Induced pluripotent stem cell lines derived from human somatic cells. *Science* 318:1917–1920.
4. Takahashi K, Okita K, Nakagawa M, Yamanaka S (2007) Induction of pluripotent stem cells from fibroblast cultures. *Nat Protoc* 2:3081–3089.
5. Takahashi K, et al. (2007) Induction of pluripotent stem cells from adult human fibroblasts by defined factors. *Cell* 131:861–872.
6. Johnson MA, Weick JP, Pearce RA, Zhang SC (2007) Functional neural development from human embryonic stem cells: accelerated synaptic activity via astrocyte coculture. *J Neurosci* 27:3069–3077.
7. Ben-Hur T, et al. (2004) Transplantation of human embryonic stem cell-derived neural progenitors improves behavioral deficit in Parkinsonian rats. *Stem Cells* 22:1246–1255.
8. Yan Y, et al. (2005) Directed differentiation of dopaminergic neuronal subtypes from human embryonic stem cells. *Stem Cells* 23:781–790.
9. Hargus G, et al. (2010) Differentiated Parkinson patient-derived induced pluripotent stem cells grow in the adult rodent brain and reduce motor asymmetry in Parkinsonian rats. *Proc Natl Acad Sci USA* 107:15921–15926.
10. Perrier AL, et al. (2004) Derivation of midbrain dopamine neurons from human embryonic stem cells. *Proc Natl Acad Sci USA* 101:12543–12548.
11. Hu BY, et al. (2010) Neural differentiation of human induced pluripotent stem cells follows developmental principles but with variable potency. *Proc Natl Acad Sci USA* 107:4335–4340.
12. Lee H, et al. (2007) Directed differentiation and transplantation of human embryonic stem cell-derived motoneurons. *Stem Cells* 25:1931–1939.
13. Li XJ, et al. (2005) Specification of motoneurons from human embryonic stem cells. *Nat Biotechnol* 23:215–221.
14. Roy NS, et al. (2006) Functional engraftment of human ES cell-derived dopaminergic neurons enriched by coculture with telomerase-immortalized midbrain astrocytes. *Nat Med* 12:1259–1268.
15. Yang D, Zhang ZJ, Oldenburg M, Ayala M, Zhang SC (2008) Human embryonic stem cell-derived dopaminergic neurons reverse functional deficit in parkinsonian rats. *Stem Cells* 26:55–63.
16. Wernig M, et al. (2008) Neurons derived from reprogrammed fibroblasts functionally integrate into the fetal brain and improve symptoms of rats with Parkinson's disease. *Proc Natl Acad Sci USA* 105:5856–5861.
17. Wu H, et al. (2007) Integrative genomic and functional analyses reveal neuronal subtype differentiation bias in human embryonic stem cell lines. *Proc Natl Acad Sci USA* 104:13821–13826.
18. Benninger F, et al. (2003) Functional integration of embryonic stem cell-derived neurons in hippocampal slice cultures. *J Neurosci* 23:7075–7083.
19. Ladewig J, et al. (2008) Lineage selection of functional and cryopreservable human embryonic stem cell-derived neurons. *Stem Cells* 26:1705–1712.
20. Koch P, Opitz T, Steinbeck JA, Ladewig J, Brüstle O (2009) A rosette-type, self-renewing human ES cell-derived neural stem cell with potential for in vitro instruction and synaptic integration. *Proc Natl Acad Sci USA* 106:3225–3230.
21. Boyden ES, Zhang F, Bamberg E, Nagel G, Deisseroth K (2005) Millisecond-timescale, genetically targeted optical control of neural activity. *Nat Neurosci* 8:1263–1268.
22. Weick JP, et al. (2010) Functional control of transplantable human ESC-derived neurons via optogenetic targeting. *Stem Cells* 28:2008–2016.
23. Peacock JH (1979) Electrophysiology of dissociated hippocampal cultures from fetal mice. *Brain Res* 169:247–260.
24. Murphy TH, Blatter LA, Wier WG, Baraban JM (1992) Spontaneous synchronous synaptic calcium transients in cultured cortical neurons. *J Neurosci* 12:4834–4845.
25. Wagenaar DA, Madhavan R, Pine J, Potter SM (2005) Controlling bursting in cortical cultures with closed-loop multi-electrode stimulation. *J Neurosci* 25:680–688.
26. Schmidt-Hieber C, Jonas P, Bischofberger J (2004) Enhanced synaptic plasticity in newly generated granule cells of the adult hippocampus. *Nature* 429:184–187.
27. Ge S, Yang CH, Hsu KS, Ming GL, Song H (2007) A critical period for enhanced synaptic plasticity in newly generated neurons of the adult brain. *Neuron* 54:559–566.
28. Espósito MS, et al. (2005) Neuronal differentiation in the adult hippocampus recapitulates embryonic development. *J Neurosci* 25:10074–10086.
29. Zhao C, Teng EM, Summers RG, Jr., Ming GL, Gage FH (2006) Distinct morphological stages of dentate granule neuron maturation in the adult mouse hippocampus. *J Neurosci* 26:3–11.
30. Jessberger S, Kempermann G (2003) Adult-born hippocampal neurons mature into activity-dependent responsiveness. *Eur J Neurosci* 18:2707–2712.
31. Toni N, et al. (2008) Neurons born in the adult dentate gyrus form functional synapses with target cells. *Nat Neurosci* 11:901–907.
32. Dunnett SB, et al. (2000) *Functional Neural Transplantation II: Novel Cell Therapies for CNS Disorders*, eds Dunnett SB, Bjorklund A (Elsevier, Amsterdam, New York).
33. Arenkiel BR, et al. (2007) In vivo light-induced activation of neural circuitry in transgenic mice expressing channelrhodopsin-2. *Neuron* 54:205–218.
34. Petreanu L, Huber D, Sobczyk A, Svoboda K (2007) Channelrhodopsin-2-assisted circuit mapping of long-range callosal projections. *Nat Neurosci* 10:663–668.
35. Zhang J, et al. (2009) Integrated device for optical stimulation and spatiotemporal electrical recording of neural activity in light-sensitized brain tissue. *J Neural Eng* 6: 055007.
36. Missale C, Nash SR, Robinson SW, Jaber M, Caron MG (1998) Dopamine receptors: from structure to function. *Physiol Rev* 78:189–225.
37. Sonntag KC, Simantov R, Isacson O (2005) Stem cells may reshape the prospect of Parkinson's disease therapy. *Brain Res Mol Brain Res* 134:34–51.
38. Maurice N, Tkatch T, Meisler M, Sprunger LK, Surmeier DJ (2001) D1/D5 dopamine receptor activation differentially modulates rapidly inactivating and persistent sodium currents in prefrontal cortex pyramidal neurons. *J Neurosci* 21:2268–2277.
39. Kim JH, et al. (2002) Dopamine neurons derived from embryonic stem cells function in an animal model of Parkinson's disease. *Nature* 418:50–56.
40. Hu X, Viesselmann C, Nam S, Merriam E, Dent EW (2008) Activity-dependent dynamic microtubule invasion of dendritic spines. *J Neurosci* 28:13094–13105.
41. Zhang F, et al. (2007) Multimodal fast optical interrogation of neural circuitry. *Nature* 446:633–639.
42. Xia X, Zhang Y, Zieth CR, Zhang SC (2007) Transgenes delivered by lentiviral vector are suppressed in human embryonic stem cells in a promoter-dependent manner. *Stem Cells Dev* 16:167–176.